Adaptive Second-Order Sliding Mode Observer-Based Fault Reconstruction for PEM Fuel Cell Air-Feed System

Salah Laghrouche, Jianxing Liu, Fayez Shakil Ahmed, Mohamed Harmouche, and Maxime Wack

***Abstract*— This paper presents an observer-based fault reconstruction method for PEM fuel cells. This method extends the results of a class of nonlinear uncertain systems with Lipschitz nonlinearities. An adaptive-gain second-order sliding mode (SOSM) observer is developed for observing the system states, where the adaptive law estimates the uncertain parameters. The inherent equivalent output error injection feature of SOSM algorithm is then used to reconstruct the fault signal. The performance of the proposed observer is validated through a hardware-in-loop emulator. The experimental results illustrate the feasibility and effectiveness of the proposed approach for application to fuel cell air-feed systems.**

***Index Terms*— Adaptive systems, fault diagnosis, fuel cells, sliding mode control.**

I. Introduction

POLYMER electrolyte membrane fuel cell (PEMFC) is an electrochemical device that produces electricity from the chemical reaction between hydrogen and oxygen. These devices are widely regarded as potential alternative power sources for stationary and mobile applications [2]. However, PEMFC systems are vulnerable to system failure or mechanical faults owing to the presence of a large number of auxiliary systems and devices required for their operation. Reliable fault detection and isolation (FDI) schemes need necessarily to be integrated in their control. FDI is achieved by residual signals, that is, differences between actual system outputs and estimated outputs obtained from dynamic models. Modeling uncertainty is a major problem in residual generation as it can also result in difference between real and modeled output. A good FDI method needs to distinguish between faults and uncertainty in the residual signals as well.

Manuscript received November 3, 2013; revised May 21, 2014 and August 4, 2014; accepted August 31, 2014. Date of publication October 30, 2014; date of current version April 14, 2015. Manuscript received in final form September 30, 2014. Recommended by Associate Editor N. K. Kazantzis *(Corresponding author: Jianxing Liu.)*

S. Laghrouche and M. Wack are with the Laboratoire OPERA, Technical University of Belfort-Montbeliard, Belfort 90010, France (e-mail: salah.laghrouche@utbm.fr; maxime.wack@utbm.fr).

J. Liu is with the Department of Control Science and Engineering, Harbin Institute of Technology, Harbin 150001, China (e-mail: jx.liu@hit.edu.cn).

F. S. Ahmed is with the Laboratory of Control and Process Engineering (LAGEP), University Claude Bernard Lyon 1, Villeurbanne 69100, France (e-mail: fahmed@lagep.univ-lyon1.fr).

M. Harmouche is with Actility, Paris 75899, France (e-mail: mohamed.harmouche@actility.com).

Color versions of one or more of the figures in this paper are available online at http://ieeexplore.ieee.org.

Digital Object Identifier 10.1109/TCST.2014.2361869

Several practical techniques exist in contemporary literature, for example, geometric approaches [3], H_∞-optimization technique [4], [5], observer-based approaches (e.g., adaptive observers [6], [7], high gain observers [8], [9], and unknown input observers [10]–[12]). Edwards and Tan [13] and Alwi and Edwards [14] proposed fault reconstruction methods which estimate the magnitude and shape of faults in addition to detection and isolation. These methods lead to active fault tolerant control (FTC) that can reconfigure the controllers to compensate the effects of faults [15].

Several observer-based FDI approaches have been studied for the fuel cell systems. Observers are important in fuel cell application as many states cannot be measured directly. Arcak *et al.* [16] developed an adaptive observer for hydrogen partial pressure estimation according to the fuel cell voltage. Görgün *et al.* [17] developed an algorithm for estimating partial pressures and the membrane water content in PEMFCs based on the resistive cell voltage drop. This algorithm has incorporated two adaptive observers for hydrogen and oxygen partial pressures, adapted from [16]. However, both of the preceding works lack robustness against the fuel cell voltage's measurement noise and the internal model relies upon unmeasurable values. Ingimundarson *et al.* [18] proposed a model-based estimation approach to hydrogen leak detection in PEMFCs without the use of relative humidity sensors. It should be noted that most of the cited papers are based on model linearization around predefined operating points of the system, depending upon the operating conditions such as temperature, humidity, and air flow. Moreover, the linearization requires calculation of Jacobian matrix of complex models such as fuel cell systems, which is time consuming, and therefore difficult in real-time implementation.

Sliding mode technique is known for its insensitivity to external disturbance due to operating conditions, high accuracy, and finite time convergence. Sliding mode observers have been widely used for fault reconstruction in the past two decades. Edwards *et al.* [19] proposed a fault reconstruction approach on the basis of equivalent output error injection. In this method, the resulting residual signal can approximate the actuator fault to any required accuracy. On the basis of the work by Edwards *et al.* [19], Tan and Edwards [20] proposed a sensor fault reconstruction method for well-modeled linear systems through the linear matrix inequality (LMI) technique. This approach is of less practical interest, as there is no explicit consideration of disturbance or uncertainty. To overcome this, Tan and Edwards [21] proposed an FDI scheme for a class of

linear systems with uncertainty, using LMI for minimizing the L_2 gain between the uncertainty and the fault reconstruction signal. Jiang *et al.* [22] proposed a sliding mode observer-based fault estimation approach for a class of nonlinear systems with uncertainties. Yan and Edwards [23] proposed a precise fault reconstruction scheme, using equivalent output error injection, for a class of nonlinear systems with uncertainty. A sufficient condition based on LMI is presented for the existence and stability of a robust sliding mode observers. This method requires a strong structural condition of the distribution associated with uncertainties. This constraint was relaxed by Yan and Edwards [1], where the fault distribution vector and the structure matrix of the uncertainty are allowed to be functions of the system's output and input. However, these works require that the bounds of the uncertainties and/or faults are *known*. Although in [1], the requirement on the bound of uncertainty is removed, it still needs to know the bound of the fault signal.

In this paper, we present a method for simultaneous state estimation, parameter identification, and fault reconstruction in PEMFC systems by extending the work in [1] to a class of nonlinear uncertain systems with Lipschitz nonlinearities. This class of systems sufficiently defines the nonlinear dynamics of the PEMFCs. The approach is based on the output injection-based fault reconstruction method presented in [19] and [24]. It involves a simple adaptive update law and an adaptive-gain SOSM observer. The uncertain parameters are estimated and then injected into an adaptive-gain SOSM observer, which maintains a sliding motion even in the presence of fault signals. Once the sliding motion is established, the equivalent output error injection can be obtained directly and used for fault reconstruction. The proposed SOSM algorithm combines the nonlinear term of the super-twisting algorithm and a linear term [25]. Lyapunov analysis demonstrates that the proposed adaptive-gain SOSM algorithm establishes ideal sliding mode without *a priori* knowledge of the upper bound of the fault signal, meanwhile, the gains of the algorithm stop increasing when the observation error converges to zero exactly.

The proposed fault reconstruction scheme is evaluated by implementing on an instrumented hardware-in-loop (HIL) test bench, which consists of a real commercial twin screw compressor and a real-time fuel cell emulation system [26]. The system states (nitrogen partial pressure and compressor speed) are estimated successfully. The stack current is estimated through the adaptive update law, considering it as an uncertainty, which eliminates the need of an extra current sensor. The fault scenario considered in this paper is a sudden air leak in the air suppply manifold, which results in a change in the outlet air flow in the supply manifold. It is reconstructed faithfully through analyzing the information, which is obtained online from comparisons between the measurements from the sensor installed in the real system and the outputs of the observer system. The phenomenon so-called oxygen starvation is monitored through the estimation of the oxygen excess ratio. The robustness of this observer against measurement noise and parameter variations is also validated experimentally.

The rest of this paper is divided as follows. The problem formulation is described in Section II. In Section III, the proposed adaptive SOSM observer is designed. In Section IV, the fault reconstruction approach is given. In Section V, the proposed adaptive SOSM observer-based fault reconstruction method is applied to the PEMFC air-feed system. The implementation and HIL experimental results are discussed in Section VI. Finally, the major conclusions are presented in Section VII.

II. Problem Formulation

Consider the following nonlinear system:

$$\dot{x} = Ax + g(x,u) + \phi(y,u)\theta + \omega(y,u)f(t), \quad y = Cx \tag{1}$$

where the matrix

$$A = \begin{bmatrix} A_1 & A_2 \\ A_3 & A_4 \end{bmatrix}, \qquad x \in \mathbb{R}^n$$

is the system state vector, $u(t) \in \mathcal{U} \subset \mathbb{R}^m$ is the control input, $y \in \mathcal{Y} \subset \mathbb{R}^p$ is the output vector, $g(x,u) \in \mathbb{R}^n$ is Lipschitz continuous, and $\phi(y,u) \in \mathbb{R}^{n\times q}$ and $\omega(y,u) \in \mathbb{R}^{n\times r}$ are assumed to be some smooth and bounded functions with $p \geq q+r$. The unknown parameter vector $\theta \in \mathbb{R}^q$ is assumed to be constant and $f(t) \in \mathbb{R}^r$ is a smooth fault signal vector, which satisfies

$$\|f(t)\| \leq \rho_1, \quad \|\dot{f}(t)\| \leq \rho_2 \tag{2}$$

where ρ_1, ρ_2 are some positive constants that might be known or unknown.

Assume that (A, C) is an observable pair, and there exists a linear coordinate transformation

$$z = Tx = \begin{bmatrix} I_p & 0 \\ -H_{(n-p)\times p} & I_{n-p} \end{bmatrix} x = \begin{bmatrix} z_1^T & z_2^T \end{bmatrix}^T$$

with $z_1 \in \mathbb{R}^p$ and $z_2 \in \mathbb{R}^{n-p}$, such that:

1) $TAT^{-1} = \begin{bmatrix} A_{11} & A_{12} \\ A_{21} & A_{22} \end{bmatrix}$, where the matrix $A_{22} = A_4 - HA_2 \in \mathbb{R}^{(n-p)\times(n-p)}$ is Hurwitz stable.
2) $CT^{-1} = [\, I_p \quad 0\,]$ where $I_p \in \mathbb{R}^{p\times p}$ is an identity matrix.

Assumption 1: There exists a function $\omega_1(y,u)$ such that

$$T\omega(y,u) = \begin{bmatrix} \omega_1(y,u) \\ 0 \end{bmatrix} \tag{3}$$

where $\omega_1(y,u) \in \mathbb{R}^{p\times r}$.

This assumption simply means that the faults only affect on the system outputs channel [1].

System (1) is described by the following equations in the new coordinate:

$$\begin{aligned} \dot{z} &= TAT^{-1}z + Tg(T^{-1}z,u) + T\phi(y,u)\theta + T\omega(y,u)f(t) \\ y &= CT^{-1}z. \end{aligned} \tag{4}$$

By reordering the state variables, system (4) can be rewritten as

$$\begin{aligned} \dot{y} &= A_{11}y + A_{21}z_2 + g_1(z_2,y,u) + \phi_1(y,u)\theta + \omega_1(y,u)f(t) \\ \dot{z}_2 &= A_{22}z_2 + A_{21}y + g_2(z_2,y,u) + \phi_2(y,u)\theta, \quad y = z_1 \end{aligned} \tag{5}$$

where

$$T\phi(y,u) = \begin{bmatrix} \phi_1(y,u) \\ \phi_2(y,u) \end{bmatrix}, \quad Tg(T^{-1}z,u) = \begin{bmatrix} g_1(z_2,y,u) \\ g_2(z_2,y,u) \end{bmatrix} \tag{6}$$

$\phi_1(\cdot,\cdot) : \mathbb{R}^p \times \mathbb{R}^m \to \mathbb{R}^p$, $\phi_2(\cdot,\cdot) : \mathbb{R}^p \times \mathbb{R}^m \to \mathbb{R}^{n-p}$, $g_1(\cdot,\cdot,\cdot) : \mathbb{R}^p \times \mathbb{R}^{n-p} \times \mathbb{R}^m \to \mathbb{R}^p$, $g_2(\cdot,\cdot,\cdot) : \mathbb{R}^p \times \mathbb{R}^{n-p} \times \mathbb{R}^m \to \mathbb{R}^{n-p}$.

In the next section, we will develop an adaptive SOSM observer for system (5), which consists of an adaptive update law and an adaptive-gain SOSM observer, to estimate the uncertain parameter and system state variables, respectively.

III. Adaptive SOSM Observer Design

Now, we consider the problem of an adaptive SOSM observer for system (5), in which the uncertain parameter is estimated with the help of an adaptive law. Then, a SOSM observer with gain adaptation is developed using the estimated parameter. Finally, with the adaptive SOSM observer, a fault reconstruction method which can be implemented online is proposed. The basic assumption on the system (5) is as follows.

Assumption 2 [1]: There exists a nonsingular matrix $\bar{T} \in \mathbb{R}^{p\times p}$, such that

$$\bar{T}\left[\phi_1(y,u)\ \omega_1(y,u)\right] = \begin{bmatrix} \Phi_1(y,u) & 0_{q\times r} \\ 0_{r\times q} & \Phi_2(y,u) \end{bmatrix} \tag{7}$$

where $\Phi_1(y,u) \in \mathbb{R}^{q\times q}$, $\Phi_2(y,u) \in \mathbb{R}^{r\times r}$ are both nonsingular matrices and bounded in $(y,u) \in \mathcal{Y}\times\mathcal{U}$.

Assumption 2 means that the uncertain parameters and the fault signals are decoupled through a nonsingular linear transformation $\bar{T}$. Let $z_y = \bar{T}y$, where $\bar{T}$ is defined in Assumption 2. Then, system (5) can be described by

$$\begin{aligned} \dot{z}_y &= \bar{T}A_{11}y + \bar{T}A_{21}z_2 + \bar{T}g_1(y,z_2,u) \\ &\quad + \begin{bmatrix} \Phi_1(y,u) \\ 0 \end{bmatrix}\theta + \begin{bmatrix} 0 \\ \Phi_2(y,u) \end{bmatrix} f(t) \\ \dot{z}_2 &= A_{22}z_2 + A_{21}y + g_2(z_2,y,u) + \phi_2(y,u)\theta \\ y &= \bar{T}^{-1}z_y \end{aligned} \tag{8}$$

where

$$\begin{aligned} \bar{T}\cdot A_{11} &= \begin{bmatrix} \bar{A}_{11} \\ \bar{A}_{12} \end{bmatrix} \\ \bar{T}\cdot A_{12} &= \begin{bmatrix} \bar{A}_{21} \\ \bar{A}_{22} \end{bmatrix} \\ \bar{T}\cdot g_1(y,z_2,u) &= \begin{bmatrix} W_{g_1}(y,z_2,u) \\ W_{g_2}(y,z_2,u) \end{bmatrix}. \end{aligned} \tag{9}$$

Let us define $z_y = [z_{y_1}\quad z_{y_2}]^T$, where $z_{y_1} \in \mathbb{R}^q, z_{y_2} \in \mathbb{R}^r$. Then, in view of (8) and (9), we obtain

$$\begin{aligned} \dot{z}_{y_1} &= \bar{A}_{11}y + \bar{A}_{21}z_2 + W_{g_1}(y,z_2,u) + \Phi_1(y,u)\theta \\ \dot{z}_{y_2} &= \bar{A}_{12}y + \bar{A}_{22}z_2 + W_{g_2}(y,z_2,u) + \Phi_2(y,u)f(t) \\ \dot{z}_2 &= A_{21}y + A_{22}z_2 + g_2(y,z_2,u) + \phi_2(y,u)\theta \\ y &= T^{-1}[z_{y_1}\quad z_{y_2}]^T. \end{aligned} \tag{10}$$

The adaptive SOSM observer is represented by the following dynamical system:

$$\begin{aligned} \dot{\hat{z}}_{y_1} &= \bar{A}_{11}y + \bar{A}_{21}\hat{z}_2 + W_{g_1}(y,\hat{z}_2,u) + \Phi_1(y,u)\hat{\theta} + \mu(e_{y_1}) \\ \dot{\hat{z}}_{y_2} &= \bar{A}_{12}y + \bar{A}_{22}\hat{z}_2 + W_{g_2}(y,\hat{z}_2,u) + \mu(e_{y_2}) \\ \dot{\hat{z}}_2 &= A_{21}y + A_{22}\hat{z}_2 + g_2(y,\hat{z}_2,u) + \phi_2(y,u)\hat{\theta} \end{aligned} \tag{11}$$

where $\mu(\cdot)$ is the output error-injection term

$$\begin{aligned} \mu(s) = \lambda(t)|s|^{\frac{1}{2}}\mathrm{sign}(s) + \ \alpha(t)\int_0^t \mathrm{sign}(s)d\tau \\ + k_\lambda(t)s + k_\alpha(t)\int_0^t s d\tau \end{aligned} \tag{12}$$

with the adaptive gains $\lambda(t)$, $\alpha(t)$, $k_\lambda(t)$, and $k_\alpha(t)$ which will be determined later on.

The observation errors are defined as $e_{y_1} = z_{y_1} - \hat{z}_{y_1}$, $e_{y_2} = z_{y_2} - \hat{z}_{y_2}$, $e_2 = z_2 - \hat{z}_2$, and $\tilde{\theta} = \theta - \hat{\theta}$. The estimate of θ, denoted by $\hat{\theta}$, is given by the following adaptive law [1]:

$$\begin{aligned} \dot{\hat{\theta}} = -K(y,u)\big(&\bar{A}_{11}y + \bar{A}_{21}\hat{z}_2 + W_{g_1}(y,\hat{z}_2,u) \\ &+ \Phi_1(y,u)\hat{\theta} - \dot{z}_{y_1}\big) \end{aligned} \tag{13}$$

where $K(y,u)$ is a positive design matrix which will be defined later.

Subtracting (11) from (10), the error dynamical equation is described by

$$\dot{e}_2 = A_{22}e_2 + \tilde{g}_2(y,z_2,\hat{z}_2,u) + \phi_2(y,u)\tilde{\theta} \tag{14}$$

$$\dot{\tilde{\theta}} = -K(y,u)\big(\bar{A}_{21}e_2 + \tilde{W}_{g_1}(y,z_2,\hat{z}_2,u) + \Phi_1(y,u)\tilde{\theta}\big) \tag{15}$$

$$\dot{e}_{y_1} = -\mu(e_{y_1}) + \bar{A}_{21}e_2 + \Phi_1(y,u)\tilde{\theta} + \tilde{W}_{g_1}(y,z_2,\hat{z}_2,u) \tag{16}$$

$$\dot{e}_{y_2} = -\mu(e_{y_2}) + \bar{A}_{22}e_2 + \Phi_2(y,u)f(t) + \tilde{W}_{g_2}(y,z_2,\hat{z}_2,u) \tag{17}$$

where $\tilde{g}_2(y,z_2,\hat{z}_2,u) = g_2(y,z_2,u) - g_2(y,\hat{z}_2,u)$, $\tilde{W}_{g_1}(y,z_2,\hat{z}_2,u) = W_{g_1}(y,z_2,u) - W_{g_1}(y,\hat{z}_2,u)$ and $\tilde{W}_{g_2}(y,z_2,\hat{z}_2,u) = W_{g_2}(y,z_2,u) - W_{g_2}(y,\hat{z}_2,u)$.

Some assumptions are imposed upon the error systems (14)–(17).

Assumption 3: The known nonlinear terms $g_2(y,z_2,u)$, $W_{g_1}(y,z_2,u)$ and $W_{g_2}(y,z_2,u)$ are Lipschitz continuous with respect to z_2

$$\begin{aligned} \|g_2(y,z_2,u) - g_2(y,\hat{z}_2,u)\| &\le \gamma_2\|z_2 - \hat{z}_2\| \\ \|W_{g_1}(y,z_2,u) - W_{g_1}(y,\hat{z}_2,u)\| &\le \gamma_{g_1}\|z_2 - \hat{z}_2\| \\ \|W_{g_2}(y,z_2,u) - W_{g_2}(y,\hat{z}_2,u)\| &\le \gamma_{g_2}\|z_2 - \hat{z}_2\| \end{aligned} \tag{18}$$

where γ_{g_1}, γ_{g_2}, and γ_2 are some known Lipschitz constants for $W_{g_1}(y,z_2,u)$, $W_{g_2}(y,z_2,u)$, and $g_2(y,z_2,u)$ respectively [27].

Given that $g(x,u)$ in (1) is Lipschitz continuous with respect to x, it follows that (18) holds under the linear transformations T and $\bar{T}$.

Assumption 4: Assume that the Hurwitz matrix A_{22} satisfies the following Riccati equation:

$$A_{22}^T P_1 + P_1 A_{22} + \gamma_2^2 P_1 P_1 + (2+\varepsilon)I_{n-p} = 0 \tag{19}$$

which has a symmetric positive-definite solution P_1 for some $\varepsilon > 0$ [28].

In other words, the matrix $A_{22} = A_4 - HA_2$ should be chosen such that (19) is satisfied.

Assumption 5: Assume that the positive design matrix $K(y,u)$ satisfies the following equation:

$$\begin{aligned} K(y,u)\Phi_1(y,u) + \Phi_1^T(y,u)K^T(y,u) - \gamma_{g_1}^2 K(y,u)K^T(y,u) \\ = \epsilon I_q \end{aligned} \tag{20}$$

for some $\epsilon > 0$.

The condition (20) is the main design consideration in this paper, and requires a design matrix $K(y,u)$ such that $K(y,u)\Phi_1(y,u) + \Phi_1^T(y,u)K^T(y,u) - \gamma_{g_1}^2 K(y,u)K^T(y,u)$ is positive definite in $(y,u) \in \mathcal{Y} \times \mathcal{U}$. Now, We will first consider the stability of the error systems (14), (15).

Theorem 1: Consider the systems (14) and (15) satisfying Assumptions 3–5. Then, the error systems (14) and (15) are exponentially stable, if for any $(y,u) \in \mathcal{Y} \times \mathcal{U}$, the following matrix:

$$Q_1 = \begin{bmatrix} \varepsilon I_{n-p}, & P_1\phi_2(y,u) - \bar{A}_{21}^T K^T(y,u) \\ \phi_2^T(y,u)P_1 - K(y,u)\bar{A}_{21}, & \epsilon I_q \end{bmatrix} \tag{21}$$

is positive definite.

Proof: The proof of this theorem follows the same steps as in [1]. A candidate Lyapunov function is chosen as

$$V_1(e_2,\tilde{\theta}) = e_2^T P_1 e_2 + \tilde{\theta}^T\tilde{\theta} \tag{22}$$

and the time derivative of V_1 along the solution of the system (14) and (15) is given by

$$\begin{aligned} \dot{V}_1 &\le e_2^T(A_{22}^T P_1 + P_1 A_{22} + \gamma_2^2 P_1 P_1 + 2I_{n-p})e_2 \\ &\quad + 2e_2^T\left(P_1\phi_2(y,u) - \bar{A}_{21}^T K^T(y,u)\right)\tilde{\theta} - \epsilon\tilde{\theta}^T\tilde{\theta} \\ &= -\begin{bmatrix} e_2^T & \tilde{\theta}^T \end{bmatrix} Q_1 \begin{bmatrix} e_2 \\ \tilde{\theta} \end{bmatrix}. \end{aligned} \tag{23}$$

Hence, the conclusion follows given that Q_1 is positive definite in $(y,u) \in \mathcal{Y} \times \mathcal{U}$. ∎

Assumption 6: It is assumed that $\|\Phi_1(y,u)\|$, $\|\Phi_2(y,u)\|$ are bounded in $(y,u) \in \mathcal{Y} \times \mathcal{U}$.

Remark 1: Theorem 1 shows that $\lim_{t\to\infty} e_2(t) = 0$ and $\lim_{t\to\infty}\tilde{\theta}(t) = 0$. Consequently, the errors $e_2, \tilde{\theta}$ and its derivatives $\dot{e}_2, \dot{\tilde{\theta}}$ are bounded. Under Assumptions 3 and 6, the time derivatives of the nonlinear terms in the error dynamics (16) and (17) are also bounded

$$\begin{aligned} \left\|\frac{d}{dt}\left(\bar{A}_{22}e_2 + \Phi_2(y,u)f(t) + \tilde{W}_{g_2}(y,z_2,\hat{z}_2,u)\right)\right\| &\le \chi_1 \\ \left\|\frac{d}{dt}\left(\bar{A}_{21}e_2 + \Phi_1(y,u)\tilde{\theta} + \tilde{W}_{g_1}(y,z_2,\hat{z}_2,u)\right)\right\| &\le \chi_2 \end{aligned} \tag{24}$$

where χ_1 and χ_2 are some unknown positive constants.
In what follows, the objective is to prove the finite time convergence of the systems (16) and (17).

Theorem 2: Assume that (24) holds and the adaptive gains $\lambda(t), \alpha(t), k_\lambda(t)$, and $k_\alpha(t)$ in the SOSM algorithm (12) are formulated as

$$\begin{aligned} \lambda(t) &= \lambda_0\sqrt{L_o(t)}, \quad \alpha(t) = \alpha_0 L_o(t) \\ k_\lambda(t) &= k_{\lambda_0}L_o(t), \quad k_\alpha(t) = k_{\alpha_0}L_o^2(t) \end{aligned} \tag{25}$$

where $\lambda_0, \alpha_0, k_{\lambda_0}$, and k_{α_0} are positive constants and $L_o(t)$ is a positive, time-varying, scalar function. The adaptive law of the time-varying function $L_o(t)$ is given by

$$\dot{L}_o(t) = \begin{cases} k, & \text{if } |e_{y_i}| \neq 0, \quad i = \{1,2\} \\ 0, & \text{else} \end{cases} \tag{26}$$

where k is an arbitrary positive value. Then, the trajectories of the error system (16) and (17) converge to zero in finite time, if λ_0, α_0, k_{λ_0}, and k_{α_0} in (25) satisfy

$$4\alpha_0 k_{\alpha_0} > 8k_{\lambda_0}^2\alpha_0 + 9\lambda_0^2 k_{\lambda_0}^2. \tag{27}$$

Proof: We only consider the proof for the system (17) and the proof for the system (16) takes the same way. The system (17) can be rewritten as

$$\begin{aligned} \dot{e}_{y_2} &= -\lambda(t)\left|e_{y_2}\right|^{\frac{1}{2}}\operatorname{sign}(e_{y_2}) - k_\lambda(t)e_{y_2} + \varphi \\ \dot{\varphi} &= -\alpha(t)\operatorname{sign}(e_{y_2}) - k_\alpha(t)e_{y_2} + \varrho(t). \end{aligned} \tag{28}$$

Under the condition (24), it follows that $\|\varrho(t)\| \le \chi_2$, where χ_2 is an *unknown* positive constant. A new state vector is introduced to represent the system (28) in a more convenient form for Lyapunov analysis

$$\zeta = \begin{bmatrix} \zeta_1 \\ \zeta_2 \\ \zeta_3 \end{bmatrix} = \begin{bmatrix} L_o^{\frac{1}{2}}(t)|e_{y_2}|^{\frac{1}{2}}\operatorname{sign}(e_{y_2}) \\ L_o(t)e_{y_2} \\ \varphi \end{bmatrix}. \tag{29}$$

Then, the system (28) can be rewritten as

$$\begin{aligned} \dot{\zeta} &= \frac{L_o(t)}{|\zeta_1|}\begin{bmatrix} -\frac{\lambda_0}{2} & 0 & \frac{1}{2} \\ 0 & -\lambda_0 & 0 \\ -\alpha_0 & 0 & 0 \end{bmatrix}\zeta \\ &\quad + L_o(t)\begin{bmatrix} -\frac{k_{\lambda_0}}{2} & 0 & 0 \\ 0 & -k_{\lambda_0} & 1 \\ 0 & -k_{\alpha_0} & 0 \end{bmatrix}\zeta + \begin{bmatrix} \frac{\dot{L}_o}{2L_o(t)}\zeta_1 \\ \frac{\dot{L}_o}{2L_o(t)}\zeta_2 \\ \varrho(t) \end{bmatrix}. \end{aligned} \tag{30}$$

Then, the following Lyapunov function candidate is introduced for the system (30):

$$V(\zeta) = \zeta^T P\zeta,\ P = \frac{1}{2}\begin{bmatrix} 4\alpha_0 + \lambda_0^2 & \lambda_0 k_{\lambda_0} & -\lambda_0 \\ \lambda_0 k_{\lambda_0} & k_{\lambda_0}^2 + 2k_{\alpha_0} & -k_{\lambda_0} \\ -\lambda_0 & -k_{\lambda_0} & 2 \end{bmatrix} \tag{31}$$

where the matrix P is symmetric positive definite due to the fact that its leading principle minors are all positive under the condition (27). Taking the derivative of (31) yields

$$\dot{V} = -L_o(t)\left(\frac{\zeta^T\Omega_1\zeta}{|\zeta_1|} + \zeta^T\Omega_2\zeta\right) + \varrho(t)q_1\zeta + \frac{q_2\dot{L}_o(t)}{L_o(t)}P\zeta \tag{32}$$

where $q_1 = \begin{bmatrix} -\lambda_0 & -k_{\lambda_0} & 2 \end{bmatrix}$, $q_2 = \begin{bmatrix} \zeta_1 & \zeta_2 & 0 \end{bmatrix}$ and

$$\begin{aligned} \Omega_1 &= \frac{\lambda_0}{2}\begin{bmatrix} \lambda_0^2 + 2\alpha_0 & 0 & -\lambda_0 \\ 0 & 2k_{\alpha_0} + 5k_{\lambda_0}^2 & -3k_{\lambda_0} \\ -\lambda_0 & -3k_{\lambda_0} & 1 \end{bmatrix} \\ \Omega_2 &= k_{\lambda_0}\begin{bmatrix} \alpha_0 + 2\lambda_0^2 & 0 & 0 \\ 0 & k_{\alpha_0} + k_{\lambda_0}^2 & -k_{\lambda_0} \\ 0 & -k_{\lambda_0} & 1 \end{bmatrix}. \end{aligned} \tag{33}$$

It is easy to verify that Ω_1 and Ω_2 are positive definite matrices under the condition (27). Because $\lambda_{\min}(P)\|\zeta\|^2 \leq V \leq \lambda_{\max}(P)\|\zeta\|^2$, (32) can be rewritten as

$$\dot{V} \leq -L_o(t)\frac{\lambda_{\min}(\Omega_1)}{\lambda_{\max}^{\frac{1}{2}}(P)}V^{\frac{1}{2}} - L_o(t)\frac{\lambda_{\min}(\Omega_2)}{\lambda_{\max}(P)}V + \frac{\chi_2\|q_1\|_2}{\lambda_{\min}^{\frac{1}{2}}(P)}V^{\frac{1}{2}} + \frac{\dot{L}_o(t)}{2L_o(t)}\zeta^T Q\zeta \tag{34}$$

where

$$Q=\begin{bmatrix} 4\alpha_0+\lambda_0^2+\lambda_0 k_{\lambda_0}+\frac{\lambda_0}{2} & 0 & 0 \\ 0 & \frac{\lambda_0+k_{\lambda_0}}{2} & 0 \\ 0 & 0 & 2k_{\alpha_0}k_{\lambda_0}^2+\lambda_0 k_{\lambda_0}+\frac{k_{\lambda_0}}{2} \end{bmatrix}. \tag{35}$$

Using (35), (34) becomes

$$\dot{V} \leq -\left(L_o(t)\gamma_1-\gamma_2\right)V^{\frac{1}{2}} - \left(L_o(t)\gamma_3-\gamma_4\frac{\dot{L}_o(t)}{L_o(t)}\right)V \tag{36}$$

where

$$\begin{aligned} \gamma_1 &= \frac{\lambda_{\min}(\Omega_1)}{\lambda_{\max}^{\frac{1}{2}}(P)} \\ \gamma_2 &= \frac{\chi_2\|q_1\|_2}{\lambda_{\min}^{\frac{1}{2}}(P)} \\ \gamma_3 &= \frac{\lambda_{\min}(\Omega_2)}{\lambda_{\max}(P)} \\ \gamma_4 &= \frac{\lambda_{\max}(Q)}{2\lambda_{\min}(P)}. \end{aligned} \tag{37}$$

Because $\dot{L}_o(t) \geq 0$ such that the terms $L_o(t)\gamma_1 - \gamma_2$ and $L_o(t)\gamma_3 - \gamma_4(\dot{L}_o(t)/L_o(t))$ are positive in finite time. It follows from (36) that

$$\dot{V} \leq -c_1 V^{\frac{1}{2}} - c_2 V \tag{38}$$

where c_1 and c_2 are positive constants. By the comparison principle, ζ converge to zero in finite time, that is, $e_{y_2} = 0$ and $\dot{e}_{y_2} = 0$. This completes the proof. ■

Remark 2: It can be seen that the adaptive law (13) depends upon $\dot{z}_{y_1}$. The adaptive-gain SOSM algorithm (12) can be used to estimate the time derivative of z_{y_1} in finite time, without requiring the bound of $|\ddot{z}_{y_1}|$ [29]. The differentiator has the following form:

$$\begin{aligned} \dot{z}_0 &= -\lambda_{0D}\sqrt{L_D(t)}|z_0 - z_{y_1}|^{\frac{1}{2}}\text{sign}(z_0 - z_{y_1}) \\ &\quad - k_{\lambda_0 D}L_D(t)(z_0 - z_{y_1}) + z_1 \\ \dot{z}_1 &= -\alpha_{0D}L_D(t)\text{sign}(z_0 - z_{y_1}) - k_{\alpha_0 D}L_D^2(t)(z_0 - z_{y_1}) \end{aligned} \tag{39}$$

where z_0 and z_1 are the real-time estimations of z_{y_1} and $\dot{z}_{y_1}$, respectively. The time-varying function $L_D(t)$ and the parameters of the differentiator λ_{0D}, $k_{\lambda_0 D}$, α_{0D}, $k_{\alpha_0 D}$ are designed as (26) and (27), respectively.

Remark 3: In view of practical implementation, the condition $|e_{y_i}| = 0$, $i = \{1, 2\}$ in (26) cannot be satisfied because of measurement noise and numerical approximations. To make the adaptive algorithm (26) practically implementable, one has to modify the condition $|e_{y_i}| = 0$ by dead-zone technique [30] as

$$\dot{L}_{o_i}(t) = \begin{cases} k, & \text{if } |\text{e}_{\text{y}_\text{i}}| \geq \tau \\ 0, & \text{else} \end{cases} \tag{40}$$

where τ is a sufficiently small positive value.

Theorems 1 and 2 have shown that systems (11) and (13) are an asymptotic state observer and uncertain parameter observer for the system (10), respectively. In the next section, we will develop the fault reconstruction approach based on those two observers.

IV. Fault Reconstruction

The fault signal $f(t)$ will be reconstructed according to the proposed observer by using an equivalent output error injection which can be obtained once the sliding surface is reached and maintained on it thereafter.

It follows from Theorem 2 that e_{y_2} and $\dot{e}_{y_2}$ in (17) are driven to zero in finite time. Thus, the equivalent output error injection can be obtained directly

$$\mu(e_{y_2}) = \bar{A}_{22}e_2 + \Phi_2(y,u)f(t) + \tilde{W}_{g_2}(y, z_2, \hat{z}_2, u). \tag{41}$$

From Assumption 2, $\Phi_2(y,u)$ is a bounded nonsingular matrix in $(y,u) \in \mathcal{Y}\times\mathcal{U}$, then the estimate of $f(t)$ can be constructed as

$$\hat{f}(t) = \Phi_2^{-1}(y,u)\mu(e_{y_2}). \tag{42}$$

Theorem 3: Suppose that conditions of Theorems (1 and 2) are satisfied, then $\hat{f}(t)$ defined in (42) is a precise reconstruction of the fault $f(t)$ because

$$\lim_{t\to\infty}\|f(t) - \hat{f}(t)\| = 0. \tag{43}$$

Proof: It follows from (41) and (42) that

$$\begin{aligned} \|f(t) - \hat{f}(t)\| &= \|\Phi_2^{-1}(y,u)\left(\bar{A}_{22}e_2 + \tilde{W}_{g_2}\right)\| \\ &\leq \|\Phi_2^{-1}(y,u)\bar{A}_{22}\|\|e_2\| + \gamma_{g_2}\|\Phi_2^{-1}(y,u)\|\|e_2\|. \end{aligned} \tag{44}$$

It follows $\lim_{t\to\infty}\|f(t) - \hat{f}(t)\| = 0$ given that $\lim_{t\to\infty}\|e_2\| = 0$. Hence, Theorem 3 is proven. ■

V. Application to PEM Fuel Cell Air-Feed Systems

Fig. 1 shows a block diagram of a typical PEM fuel cell system in automotive applications, which consists of four major subsystems: the air-feed subsystem, the hydrogen supply subsystem, the humidify subsystem and the cooling subsystem. The PEMFCs are supplied at the cathode with compressed air via a supply manifold. The compressor draws the air from the atmosphere directly. At the cathode exit, the air enters an outlet manifold that is open to the atmosphere. Several assumptions are made for the system. Mainly, the anode pressure is assumed to be well controlled and equal to the cathode pressure [31]. The input reactant flows are humidified in a consistent and rapid way and the

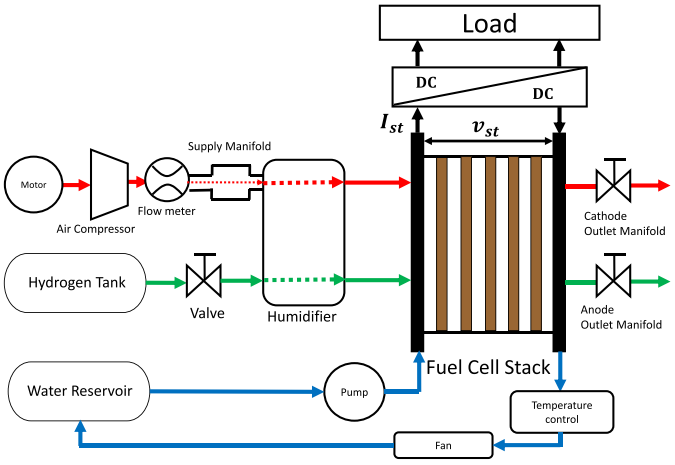

Fig. 1. Fuel cell system scheme.

high-pressure compressed hydrogen is available. Vapor partial pressure in the stack is considered equal to the saturation pressure.

The dynamic of the cathode pressure proposed in [32] is used in our model. The state space representation of this model is as follows:

$$\begin{aligned}
\dot{x}_1 &= -(c_1+c_8)(x_1-x_4) - \frac{c_3(x_1-c_2)}{\kappa x_1} W_{\text{ca,out}} - c_7\xi \\
\dot{x}_2 &= c_8(x_4-x_1) - \frac{c_3 x_2}{\kappa x_1} W_{\text{ca,out}} \\
\dot{x}_3 &= -c_9 x_3 - \frac{c_{10}}{x_3}\left[\left(\frac{x_4}{c_{11}}\right)^{c_{12}} - 1\right] W_{\text{cp}} + c_{13}u \\
\dot{x}_4 &= c_{14}\left[1 + c_{15}\left[\left(\frac{x_4}{c_{11}}\right)^{c_{12}} - 1\right]\right] \times \left[W_{\text{cp}} - c_{16}(x_4 - x_1)\right]
\end{aligned} \tag{45}$$

where $x_1 := p_{\text{cp}}$ is the cathode pressure, $x_2 := p_{N_2}$ is the nitrogen partial pressure, $x_3 := \omega_{\text{cp}}$ is the compressor speed, and $x_4 := p_{\text{sm}}$ is the supply manifold pressure. $W_{\text{ca,out}}$ is the cathode flow rate which is a function of the cathode pressure $W_{\text{ca,out}} = k_{\text{ca,out}}(p_{\text{ca}} - p_{\text{atm}})^{1/2}$ and W_{cp} is the compressor flow rate which is a function of the angular speed of the compressor $W_{\text{cp}} = h_3(x_3) = c_{17}\omega_{\text{cp}}$ [26]. The stack current ξ is considered as an uncertain parameter θ. The control input u represents the motor's quadratic current component. The cathode and supply manifold pressures are assumed to be available for measurement. Thus, the system outputs are $y = [x_1 \;\; x_4]^T$. The system performance variable, oxygen excess ratio λ_{O_2} is defined as the ratio between the oxygen entering the cathode $W_{O_2,\text{in}}$ and the oxygen reacting in the fuel cell stack $W_{O_2,\text{react}}$

$$\lambda_{O_2} = \frac{W_{O_2,\text{in}}}{W_{O_2,\text{react}}} = \frac{c_{18}(x_4 - x_1)}{c_{19}\xi}. \tag{46}$$

Because of safety and high efficiency, it is typical to operate the stacks with this value equals 2 during step changes of load current demand [26]. It should be noted that positive deviations of λ_{O_2} above 2 imply lower efficiency, because excess oxygen supplied into the cathode will cause power waste, and negative deviations increase the probability of the starvation phenomena. We consider a fault scenario: a sudden air leak in the air supply manifold. This fault is simulated with an increment Δc_{16} in the supply manifold outlet flow constant $c_{16} := k_{\text{sm,out}}$, which is translated into a change in the outlet air flow in the supply manifold $W_{\text{sm,out}} = (c_{16}+\Delta c_{16})(x_4 - x_1)$ [33], [34]. We assume that this fault appears after time $t = 50$ s, that is, $\Delta c_{16} = 0.2c_{16}$. Thus, the fault signal $f(t)$ appears in the output channel x_4 is defined as

$$f(t) = \begin{cases} \Delta c_{16} \times (x_4 - x_1) \text{ kg/s}, & \text{if } t \geq 50 \text{ s} \\ 0, & \text{else.} \end{cases} \tag{47}$$

All the parameters $c_i, i \in \{1, \ldots, 19\}$ are positive and depend on the physical values of the fuel cell (Appendix).

To design the proposed observer for the fuel cell system, let us define $z_{y_1} := x_1$, $z_{y_2} := x_4$, $z_2 := [x_2 \;\; x_3]^T$, and $\theta := \xi$. Then, system (45) is described as the form of (10)

$$\begin{aligned}
\dot{z}_{y_1} &= -(c_1+c_8)(z_{y_1} - z_{y_2}) - \frac{c_3(z_{y_1}-c_2)W_{\text{ca,out}}}{\kappa z_{y_1}} - c_4\theta \\
\dot{z}_{y_2} &= c_{14}\left[1 + c_{15}\left[\left(\frac{z_{y_2}}{c_{11}}\right)^{c_{12}} - 1\right]\right] \\
&\quad \times \left[h_3(D_2 z_2) - (c_{16} + \Delta c_{16})(z_{y_2} - z_{y_1})\right] \\
\dot{z}_2 &= \underbrace{\begin{bmatrix} -H & 0 \\ 0 & -c_9 \end{bmatrix}}_{A_{22}} z_2 + \underbrace{\begin{bmatrix} -c_8 & c_8 \\ 0 & 0 \end{bmatrix}}_{A_{21}} y \\
&\quad + \underbrace{\begin{bmatrix} D_1 z_2 \left(H - \dfrac{c_3 W_{\text{ca,out}}}{\kappa z_{y_1}}\right) \\ -\dfrac{c_{10}}{D_2 z_2}\left[\left(\dfrac{z_{y_2}}{c_{11}}\right)^{c_{12}} - 1\right] h_3(D_2 z_2) + c_{13}u \end{bmatrix}}_{g_2(y,z_2,u)}
\end{aligned} \tag{48}$$

where

$$\begin{aligned}
&D_1 = [1, 0], \;\; D_2 = [0, 1], \Phi_1(y,u) := -c_4, \Phi_2(y,u) := c_5 \\
&W_{g_1}(y, z_2, u) := -\frac{c_3(z_{y_1} - c_2)\psi(z_{y_1})}{\kappa z_{y_1}}, \;\; \phi_2(y,u) = 0 \\
&W_{g_2}(y, z_2, u) := c_{14}c_{15}\left(\frac{z_{y_2}}{c_{11}}\right)^{c_{12}} \left(h_3(D_2 z_2) - c_{16}(z_{y_2} - z_{y_1})\right)
\end{aligned}$$

and the design parameter H is chosen to satisfy the Riccati equation (19). The fault signal is weighted by c_5, modeled as

$$c_5 = -c_{14}\left[1 + c_{15}\left[\left(\frac{z_{y_2}}{c_{11}}\right)^{c_{12}} - 1\right]\right]. \tag{49}$$

The adaptive-gain SOSM observer for the system (48) is designed as the form (11) and (13)

$$\begin{aligned}
\dot{\hat{z}}_{y_1} &= -(c_1+c_8)(z_{y_1} - z_{y_2}) - \frac{c_3(z_{y_1}-c_2)}{\kappa z_{y_1}} W_{\text{ca,out}} - c_4\hat{\theta} + \mu(e_{y_1}) \\
\dot{\hat{z}}_{y_2} &= c_{14}\left[1 + c_{15}\left[\left(\frac{z_{y_2}}{c_{11}}\right)^{c_{12}} - 1\right]\right] \\
&\quad \times \left[h_3(D_2\hat{z}_2) - c_{16}(z_{y_2} - z_{y_1})\right] + \mu(e_{y_2}) \\
\dot{\hat{z}}_2 &= A_{22}\hat{z}_2 + A_{21}y + g_2(y, \hat{z}_2, u)
\end{aligned} \tag{50}$$

and

$$\begin{aligned}
\dot{\hat{\theta}} = -K\Bigg(&c_4\hat{\theta} + (c_1+c_8)(z_{y_1} - z_{y_2}) \\
&+ \frac{c_3(z_{y_1}-c_2)W_{\text{ca,out}}}{\kappa z_{y_1}} + \dot{z}_{y_1}\Bigg)
\end{aligned} \tag{51}$$

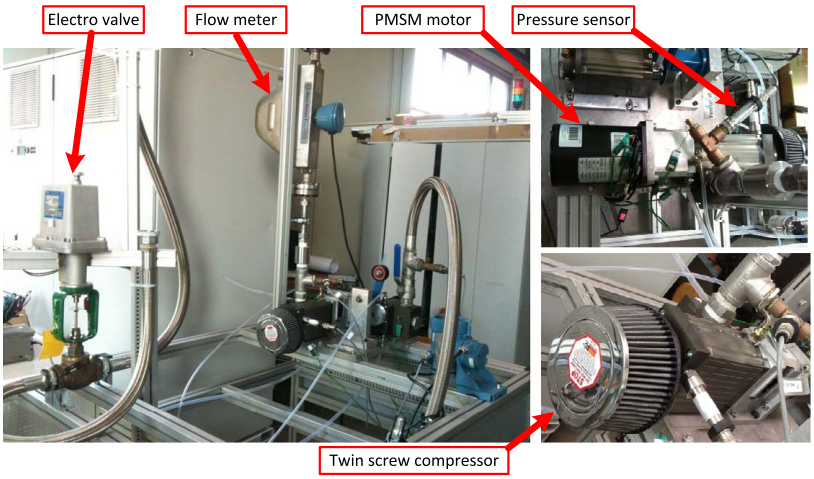

Fig. 2. Test bench.

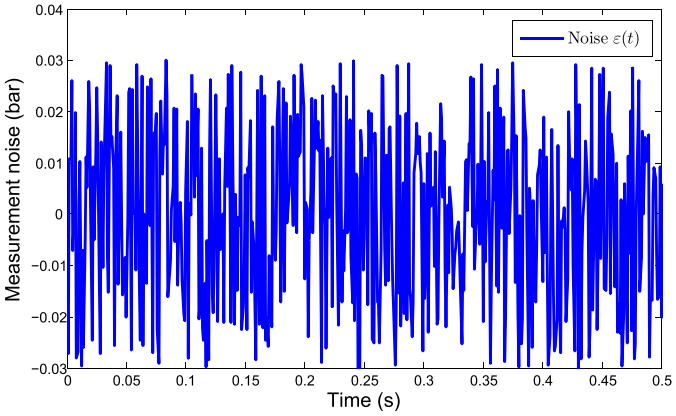

Fig. 3. System output measurement noise.

where $e_{y_1} = z_{y_1} - \hat{z}_{y_1}$, $e_{y_2} = z_{y_2} - \hat{z}_{y_2}$ and the adaptive gains of the SOSM algorithm $\mu(e_{y_1})$, $\mu(e_{y_2})$ are designed according to (25) and (26). The value of $\dot{z}_{y_1}$ is obtained from the robust exact finite time differentiator (39) in [35].

The oxygen excess ratio λ_{O_2} and the fault signal $f(t)$ are estimated

$$\hat{\lambda}_{O_2} = \frac{c_{18}(x_4 - x_1)}{c_{19}\hat{\theta}}, \quad \hat{f}(t) = \frac{\mu(e_{y_2})}{c_5}. \tag{52}$$

Remark 4: The Assumptions 3 and 6 are satisfied by the functions $W_{g_1}(y, z_2, u)$, $W_{g_2}(y, z_2, u)$, $\Phi_1(y, u)$, $\Phi_2(y, u)$, and $g_2(y, z_2, u)$. The Riccati equation in Assumption 4 is satisfied by appropriate value of the design gain $H = 0.5$. Assumption 5 is also satisfied for some $\epsilon = 0.02$, because the (20) is simplified into a scalar equation.

VI. Experimentation

Experiments have been performed on a HIL test bench shown in Fig. 2. It consists of a physical air-feed system, based on a commercial twin screw compressor, and a real-time fuel cell emulator. The twin screw compressor consists of two helical rotors which are coupled directly to its motor. Air intake is at the opposite side of the mechanical transmission and the output pressure is regulated by a servo valve. It has a flow rate margin 0–0.1 kg/s at a maximum velocity of 12 000 r/min.

TABLE I
Variations of System Parameters

Symbol	Parameter	Value
n	Number of cells in stack	90
R	Universal gas constant	8.314 J/(mol K)
T_{fc}	Temperature of the fuel cell	353.15 K
F	Faraday constant	96485 C/mol
p_{atm}	Atmospheric pressure	1.01325 $\times 10^5$ Pa
T_{atm}	Atmospheric temperature	298.15 K
V_{ca}	Cathode volume	0.0015 m^3
V_{sm}	Supply manifold volume	0.003 m^3
$k_{ca,in}$	Cathode inlet constant	0.3629×10^{-5}kg/(Pa s)
$k_{ca,out}$	Cathode outlet constant	0.76×10^{-4}kg/(Pa s)
$k_{sm,out}$	Supply manifold outlet constant	0.3629×10^{-5}kg/(Pa s)
$x_{O_2,atm}$	Oxygen mass fraction	0.23
M_a	Air molar mass	28.9644×10^{-3} kg/mol
M_{O_2}	Oxygen molar mass	32×10^{-3} kg/mol
M_{N_2}	Nitrogen molar mass	28×10^{-3} kg/mol
γ	Ratio of specific heats of air	1.4
C_p	Specific heat capacity of air	1004 J/(kg K)
J_{cp}	Compressor inertia	671.9 $\times10^{-5}$ kg m^2
η_{cp}	Compressor efficiency	80%
η_{cm}	Motor mechanical efficiency	98%
k_t	Motor constant	0.31 N m/A
f	Motor friction	0.00136 V/(rad/s)
$V_{cpr/tr}$	Compressor volume per turn	$5\times10^{-4}\mathrm{m}^3$/tr
ρ_a	Air density	1.23 kg/m^3
μ	Smoothing filter time constant	0.01 s
$L(0)$	Initial value of $L(t)$	5
k	Design parameter in (26)	10

TABLE II
Emulated PEMFC System Parameters

Symbol	Parameter	Value
T_{fc}	Temperature of the fuel cell, $^\circ$C	+10%
V_{ca}	Cathode volume, m^3	+10%
V_{sm}	Supply manifold volume, m^3	-10%
T_{atm}	Ambient temperature, $^\circ$C	+10%
$k_{ca,in}$	Cathode inlet orifice constant, kg/(Pa·s)	+5%
$k_{ca,out}$	Cathode outlet orifice constant, kg/(Pa·s)	+5%

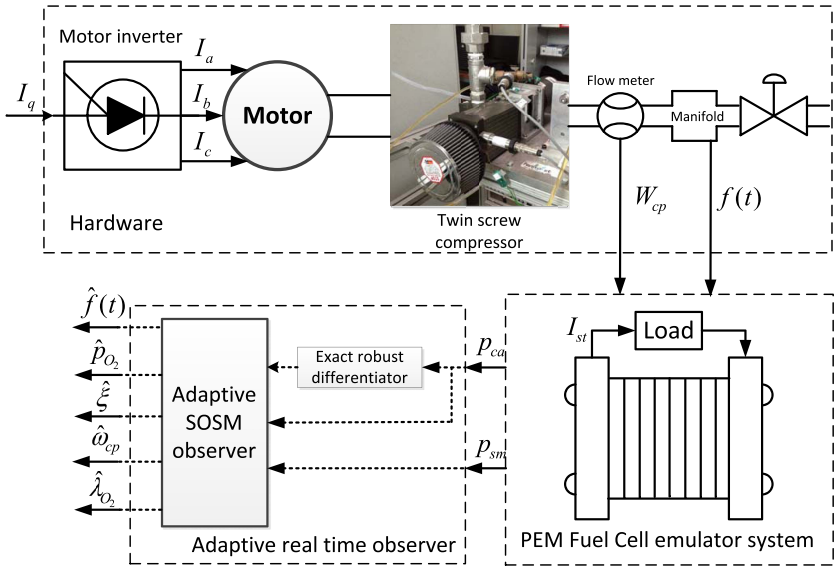

Fig. 4. Schematic diagram of the observer-based fault reconstruction.

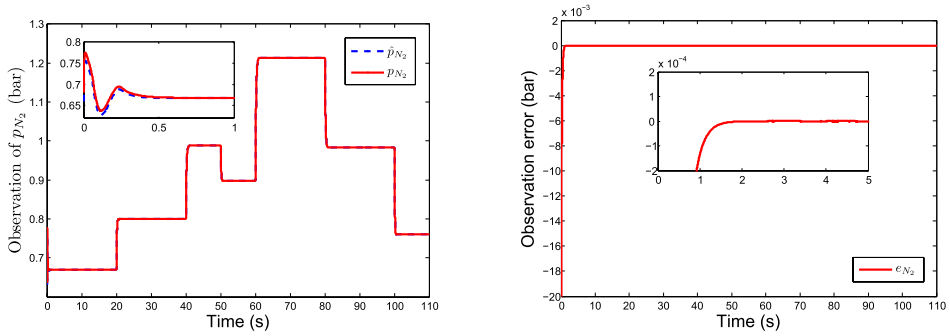

(a) (b)

Fig. 5. Estimate of nitrogen partial pressure and its error. (a) Estimate of p_{N_2}. (b) Estimation error e_{N_2}.

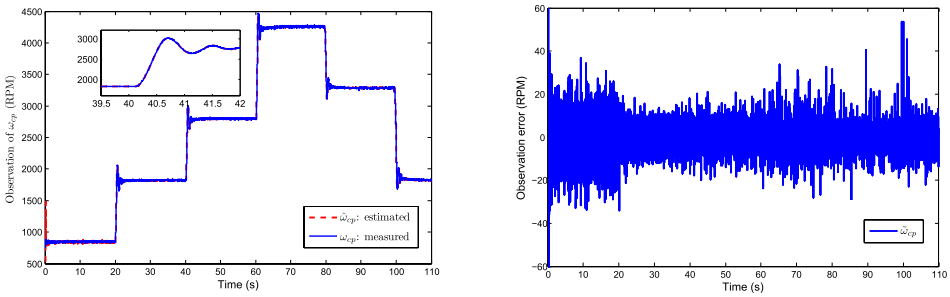

(a) (b)

Fig. 6. Estimate of compressor speed and its error. (a) Estimate and measurement of ω_{cp}. (b) Estimation error $\tilde{\omega}_{\mathrm{cp}}$.

The compressor is driven by a permanent magnet synchronous motor through an inverter controlled by three-phase currents I_a, I_b, and I_c. The quadratic current I_q is generated by the robust suboptimal SOSM controller presented in [26], which is implemented on National Instruments CompactRIO real-time control system.

A. PEMFC Emulator

To avoid excessive hydrogen consumption while working on PEMFC auxiliary systems, the laboratory has designed an emulator. The advantage of this emulator is that it provides an economical as well as safer alternative for real-time experiments that do not require the fuel cell core reaction. The emulator is based on the specifications of a 90-cell 33 kW commercial PEMFC unit and runs at a clock frequency of 40 MHz and an overall loop frequency of 10 kHz. The emulator parameters can be varied through software, to perform stability and robustness tests. The PEMFC emulator runs a detailed ninth-order dynamic model

$$x = [p_{O_2},\ p_{H_2},\ p_{N_2},\ p_{\mathrm{sm}},\ m_{\mathrm{sm}},\ p_{v,\mathrm{an}},\ p_{v,\mathrm{ca}},\ p_{\mathrm{rm}},\ T_{\mathrm{st}}]^T \tag{53}$$

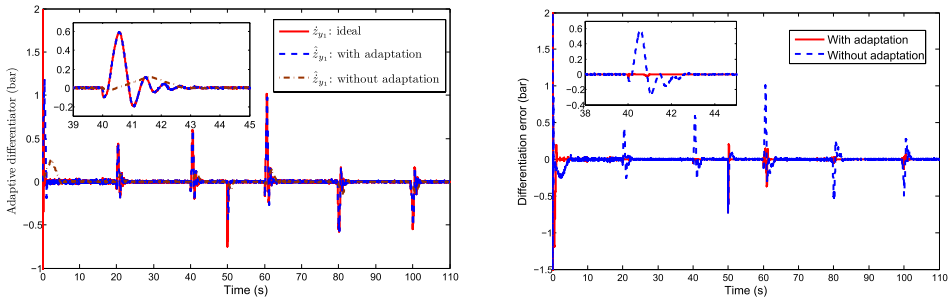

(a) (b)

Fig. 7. Comparison between Levant's fixed gain differentiator and adaptive super twisting differentiator. (a) Differentiation of z_{y_1}. (b) Differentiation error of z_{y_1}.

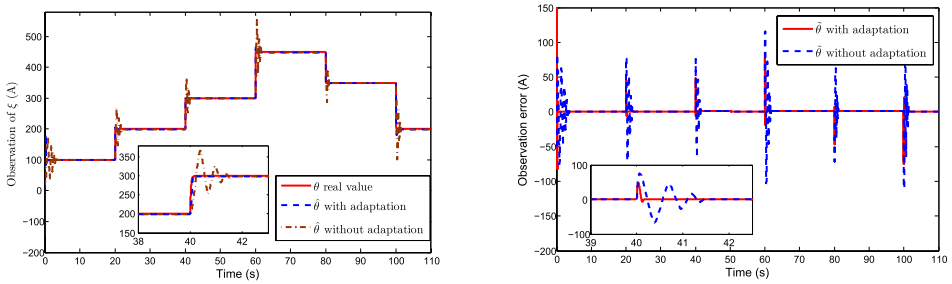

(a) (b)

Fig. 8. Estimate of stack current and its error (using Levant's fixed gain differentiator and adaptive super twisting differentiator). (a) Estimate of θ. (b) Error in estimation $\tilde{\theta}$.

where p_{H_2} is the hydrogen pressure in the anode, m_{sm} is the mass of air in supply manifold, $p_{v,\text{an}}$ is the vapor partial pressure in the anode, $p_{v,\text{ca}}$ is the vapor partial pressure in the cathode, p_{rm} is the pressure of return manifold, and T_{st} is the stack temperature. This dynamic model is based on Pukrushpan *et al.* [36], with the added temperature model described by

$$\begin{aligned} m_{\text{st}} C_{p_{\text{st}}} \frac{dT_{\text{st}}}{dt} &= \dot{Q}_{\text{sou}} - W_c C_{p_c} \left(T_{\text{st}} - T_{c,\text{in}}\right) \\ \dot{Q}_{\text{sou}} &= I_{\text{st}} \left(-\frac{T\,\Delta s}{4F} + v_{\text{act}} + I_{\text{st}} R_{\text{ohm}}\right) \end{aligned} \tag{54}$$

where m_{st} is the heat mass of the stack, $C_{p_{\text{st}}}$ and C_{p_c} are the specific heat, W_c is the coolant flow rate considered as a control variable, $T_{c,\text{in}}$ is the coolant temperature at the stack inlet, and $\dot{Q}_{\text{sou}}$ is the internal energy source. The PEMFC works under several safety constraints, such as minimum pressure difference between the anode and cathode and regulated stack temperature. The stack voltage output of the PEMFC emulator is computed using the following equation:

$$V_{\text{st}} = n(E - v_{\text{act}} - v_{\text{ohm}} - v_{\text{conc}}) \tag{55}$$

where n is the number of cells, E is the open circuit voltage, v_{act} is the activation loss at catalyst layer (V), v_{ohm} is the ohmic loss, and v_{conc} is the concentration loss. The open circuit voltage E can be obtained from the Nernst equation for fuel cells. The ohmic loss is due to the membrane resistance, expressed as $v_{\text{ohm}} = i R_{\text{ohm}}$. The concentration loss is approximated as $v_{\text{conc}} = i(b_3 i / i_{\max})^{b_4}$, where b_3, b_4, and $i_{\max}$ are constants that depend on the temperature and the reactant partial pressures.

B. Experimental Results

The structure of the observer-based fault reconstruction strategy is shown in Fig. 3. The nominal values of the parameters for the HIL emulator are shown in Table I. To test the robustness of the proposed observer-based fault reconstruction approach against parametric uncertainty, the system parameters, such as temperatures, volumes, cathode inlet and outlet orifice, motor constant, and compressor inertia, have been varied around their nominal values according to the worst case percentages, are given in Table II.

During the tests, the stack current varied between 100 and 450 A, corresponding to flow rate variation in the compressor between 7 and 28 g/s. The measurement noise was also included to test the robustness of the proposed approach, that is, $y_1 = p_{\text{ca}} + \epsilon(t)$, $y_2 = p_{\text{sm}} + \epsilon(t)$, where $\epsilon(t)$ is the measurement noise as shown in Fig. 4. The state observations $(p_{N_2}, \omega_{\text{cp}})$ in response to steps changes in the load current are shown in Figs. 5 and 6. It can be seen from these figures that the settling time of both upward load changes (i.e., $t = 40$ s, $t = 60$ s) and downward load changes (i.e., $t = 80$ s, $t = 100$ s) is less than 2 s. It should be pointed out that the estimate of compressor speed is compared with experimental measurement.

The outputs of the adaptive differentiator and Levant's fixed gain differentiator [35] are shown in Fig. 7. It is easy to see that the proposed adaptive differentiator has faster convergence and

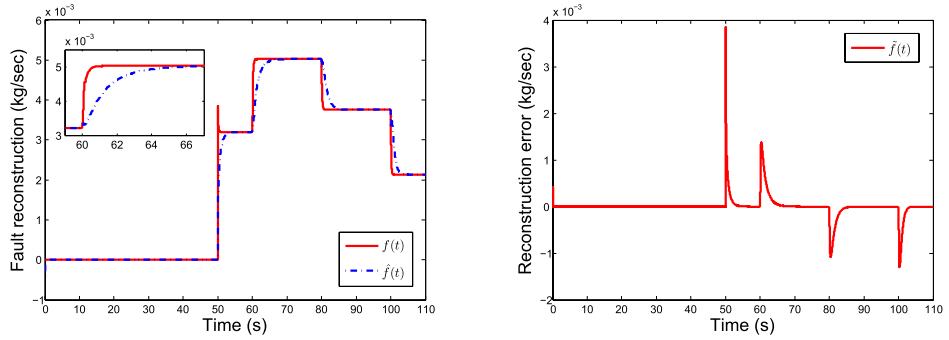

(a) (b)

Fig. 9. Fault reconstruction and its error. (a) Estimate of $f(t)$. (b) Estimation error $\tilde{f}(t)$.

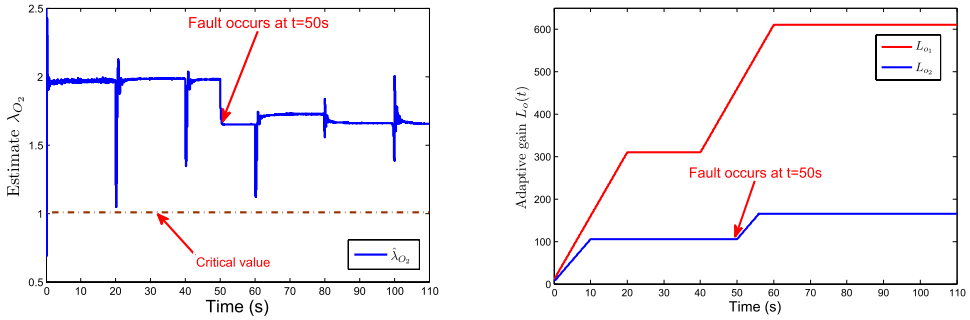

(a) (b)

Fig. 10. Estimate of λ_{O_2} and gain $L_o(t)$ versus time (s). (a) Estimate of oxygen excess ratio. (b) Adaptive law of $L_o(t)$.

less overshoot. Fig. 8 shows the estimate of the stack current, as an unknown parameter θ, based on the adaptive law. Both, the result obtained from application of Levant's differentiator and the adaptive differentiator are presented. It can be seen that the adaptive differentiator improves the performance of the adaptive law and gives a good estimate for the stack current. The fault signal is reconstructed faithfully as shown in Fig. 9. It is clear that the proposed scheme is capable of reconstructing fault signal and state estimation simultaneously in the presence of uncertain parameter. The estimate of oxygen excess ratio is shown in Fig. 10(a). It is easy to see that this value decreases after $t = 50$ s. This is due to the occurrence of the fault (air leak in the supply manifold) after $t = 50$ s. In this case, the air flow supplied by the compressor needs to increase, taking into account the effect of the fault, to ensure safe operation of the fuel cell. The time history of the adaptive-gain $L_o(t)$ is shown in Fig. 10(b), where the exponential convergence of the observer is ensured. The gains of the SOSM algorithm stop increasing when the output observation error converges to zero in finite time.

VII. Conclusion

This paper has proposed a robust fault reconstruction method for a class of nonlinear uncertain systems with Lipschitz nonlinearities on the basis of an adaptive SOSM observer. An adaptive update law has been given to identify the uncertain parameter. The estimated parameter is then injected into an adaptive-gain SOSM observer, which maintains a sliding motion in the presence of the fault signal. The proposed fault reconstruction approach was successfully implemented on a HIL test bench. The fault scenario of a sudden air leak in the supply manifold was reconstructed precisely. The experimental results have shown that the proposed approach is effective and feasible. In the future, other faults such as drying or flooding at the cell stack and starvation will be considered.

Appendix

$$c_1 = \frac{RT_{\text{fc}}k_{\text{ca,in}}}{M_{O_2}V_{\text{ca}}}\left(\frac{x_{O_2,atm}}{1+\omega_{\text{ca,in}}}\right);\quad c_2 = p_{\text{sat}};\quad c_3 = \frac{RT_{\text{fc}}}{V_{\text{ca}}}$$

$$c_7 = \frac{nRT_{\text{fc}}}{4FV_{\text{ca}}};\quad c_8 = \frac{RT_{\text{fc}}k_{\text{ca,in}}}{M_{N_2}V_{\text{ca}}}\left(\frac{1-x_{O_2,\text{atm}}}{1+\omega_{\text{atm}}}\right);\quad c_9 = \frac{f}{J_{\text{cp}}}$$

$$c_{10} = \frac{C_pT_{\text{atm}}}{J_{\text{cp}}\eta_{\text{cp}}};\quad c_{11} = p_{\text{atm}};\quad c_{12} = \frac{\gamma-1}{\gamma}$$

$$c_{13} = \frac{\eta_{\text{cm}}k_t}{J_{\text{cp}}};\quad c_{14} = \frac{\gamma\, RT_{\text{atm}}}{M_aV_{\text{sm}}};\quad c_{15} = \frac{1}{\eta_{\text{cp}}}$$

$$c_{16} = k_{\text{sm,out}};\quad c_{17} = \frac{1}{2\pi}\eta_{v-c}V_{\text{cpr/tr}}\rho_a;$$

$$c_{18} = k_{\text{ca,in}}\frac{x_{O_2,\text{atm}}}{1+\omega_{\text{ca,in}}};\quad c_{19} = \frac{nM_{O_2}}{4F}$$

References

[1] X.-G. Yan and C. Edwards, "Adaptive sliding-mode-observer-based fault reconstruction for nonlinear systems with parametric uncertainties," *IEEE Trans. Ind. Electron.*, vol. 55, no. 11, pp. 4029–4036, Nov. 2008.

[2] L. Carrette, K. A. Friedrich, and U. Stimming, "Fuel cells—Fundamentals and applications," *Fuel Cells*, vol. 1, no. 1, pp. 5–39, 2001.

[3] C. De Persis and A. Isidori, "A geometric approach to nonlinear fault detection and isolation," *IEEE Trans. Autom. Control*, vol. 46, no. 6, pp. 853–865, Jun. 2001.

[4] Z. Qiu and J. Gertler, "Robust FDI systems and H_∞-optimization-disturbances and tall fault case," in *Proc. 32nd IEEE Conf. Decision Control*, San Antonio, TX, USA, Dec. 1993, pp. 1710–1715.
[5] M. Hou and R. J. Patton, "An LMI approach to H_-/H_∞ fault detection observers," in *Proc. UKACC Int. Conf. Control*, Sep. 1996, pp. 305–310.
[6] H. Yang and M. Saif, "Nonlinear adaptive observer design for fault detection," in *Proc. Amer. Control Conf.*, Jun. 1995, pp. 1136–1139.
[7] H. Wang, Z. J. Huang, and S. Daley, "On the use of adaptive updating rules for actuator and sensor fault diagnosis," *Automatica*, vol. 33, no. 2, pp. 217–225, 1997.
[8] G. Besançon, "High-gain observation with disturbance attenuation and application to robust fault detection," *Automatica*, vol. 39, no. 6, pp. 1095–1102, 2003.
[9] K. C. Veluvolu, M. Defoort, and Y. C. Soh, "High-gain observer with sliding mode for nonlinear state estimation and fault reconstruction," *J. Franklin Inst.*, vol. 351, no. 4, pp. 1995–2014, 2013.
[10] M. Hou and P. C. Muller, "Design of observers for linear systems with unknown inputs," *IEEE Trans. Autom. Control*, vol. 37, no. 6, pp. 871–875, Jan. 1992.
[11] J. Chen, R. J. Patton, and H.-Y. Zhang, "Design of unknown input observers and robust fault detection filters," *Int. J. Control*, vol. 63, no. 1, pp. 85–105, 1996.
[12] J. Chen and R. J. Patton, "Robust residual generation using unknown input observers," in *Robust Model-Based Fault Diagnosis for Dynamic Systems*, vol. 3. Norwell, MA, USA: Kluwer, 1999, pp. 65–108.
[13] C. Edwards and C. P. Tan, "Sensor fault tolerant control using sliding mode observers," *Control Eng. Pract.*, vol. 14, no. 8, pp. 897–908, 2006.
[14] H. Alwi and C. Edwards, "Fault detection and fault-tolerant control of a civil aircraft using a sliding-mode-based scheme," *IEEE Trans. Control Syst. Technol.*, vol. 16, no. 3, pp. 499–510, May 2008.
[15] Y. Zhang and J. Jiang, "Bibliographical review on reconfigurable fault-tolerant control systems," *Ann. Rev. Control*, vol. 32, no. 2, pp. 229–252, 2008.
[16] M. Arcak, H. Gorgun, L. M. Pedersen, and S. Varigonda, "A nonlinear observer design for fuel cell hydrogen estimation," *IEEE Trans. Control Syst. Technol.*, vol. 12, no. 1, pp. 101–110, Jan. 2004.
[17] H. Görgün, M. Arcak, and F. Barbir, "An algorithm for estimation of membrane water content in PEM fuel cells," *J. Power Sour.*, vol. 157, no. 1, pp. 389–394, 2006.
[18] A. Ingimundarson, A. G. Stefanopoulou, and D. A. McKay, "Model-based detection of hydrogen leaks in a fuel cell stack," *IEEE Trans. Control Syst. Technol.*, vol. 16, no. 5, pp. 1004–1012, Jul. 2008.
[19] C. Edwards, S. K. Spurgeon, and R. J. Patton, "Sliding mode observers for fault detection and isolation," *Automatica*, vol. 36, no. 4, pp. 541–553, 2000.
[20] C. P. Tan and C. Edwards, "Sliding mode observers for detection and reconstruction of sensor faults," *Automatica*, vol. 38, no. 10, pp. 1815–1821, 2002.
[21] C. P. Tan and C. Edwards, "Sliding mode observers for robust detection and reconstruction of actuator and sensor faults," *Int. J. Robust Nonlinear Control*, vol. 13, no. 5, pp. 443–463, 2003.
[22] B. Jiang, M. Staroswiecki, and V. Cocquempot, "Fault estimation in nonlinear uncertain systems using robust/sliding-mode observers," *IEE Proc.-Control Theory Appl.*, vol. 151, no. 1, pp. 29–37, Jan. 2004.
[23] X.-G. Yan and C. Edwards, "Nonlinear robust fault reconstruction and estimation using a sliding mode observer," *Automatica*, vol. 43, no. 9, pp. 1605–1614, 2007.
[24] S. K. Spurgeon, "Sliding mode observers: A survey," *Int. J. Syst. Sci.*, vol. 39, no. 8, pp. 751–764, 2008.
[25] J. A. Moreno and M. Osorio, "A Lyapunov approach to second-order sliding mode controllers and observers," in *Proc. 47th IEEE Conf. Decision Control*, Dec. 2008, pp. 2856–2861.
[26] I. Matraji, S. Laghrouche, S. Jemei, and M. Wack, "Robust control of the PEM fuel cell air-feed system via sub-optimal second order sliding mode," *Appl. Energy*, vol. 104, pp. 945–957, Apr. 2013.
[27] X. Zhang, M. Polycarpou, and T. Parisini, "Fault diagnosis of a class of nonlinear uncertain systems with Lipschitz nonlinearities using adaptive estimation," *Automatica*, vol. 46, no. 2, pp. 290–299, 2010.
[28] R. Rajamani, "Observers for Lipschitz nonlinear systems," *IEEE Trans. Autom. Control*, vol. 43, no. 3, pp. 397–401, Mar. 1998.
[29] J. Liu, S. Laghrouche, and M. Wack, "Differential flatness-based observer design for a PEM fuel cell using adaptive-gain sliding mode differentiators," in *Proc. Eur. Control Conf. (ECC)*, Jul. 2013, pp. 2477–2482.
[30] A. Pisano and E. Usai, "Globally convergent real-time differentiation via second order sliding modes," *Int. J. Syst. Sci.*, vol. 38, no. 10, pp. 833–844, 2007.
[31] J. T. Pukrushpan, A. G. Stefanopoulou, and H. Peng, *Control of Fuel Cell Power Systems: Principles, Modeling, Analysis and Feedback Design*. New York, NY, USA: Springer-Verlag, 2004.
[32] R. J. Talj, D. Hissel, R. Ortega, M. Becherif, and M. Hilairet, "Experimental validation of a PEM fuel-cell reduced-order model and a moto-compressor higher order sliding-mode control," *IEEE Trans. Ind. Electron.*, vol. 57, no. 6, pp. 1906–1913, Jun. 2010.
[33] T. Escobet *et al.*, "Model-based fault diagnosis in PEM fuel cell systems," *J. Power Sour.*, vol. 192, no. 1, pp. 216–223, 2009.
[34] S. de Lira, V. Puig, J. Quevedo, and A. Husar, "LPV observer design for PEM fuel cell system: Application to fault detection," *J. Power Sour.*, vol. 196, no. 9, pp. 4298–4305, 2011.
[35] A. Levant, "Robust exact differentiation via sliding mode technique," *Automatica*, vol. 34, no. 3, pp. 379–384, 1998.
[36] J. T. Pukrushpan, A. G. Stefanopoulou, and H. Peng, "Control of fuel cell breathing," *IEEE Control Syst.*, vol. 24, no. 2, pp. 30–46, Apr. 2004.

Salah Laghrouche received the Electrical Engineering degree from the University of Algiers, Algiers, Algeria, in 2001, and the Ph.D. degree from the Central School of Nantes, Nantes, France, in 2004, where he received a scholarship to undertake research in nonlinear control.

He joined the Signals and Systems Laboratory at the National Center for Scientific Research, Supélec, University Paris-Sud, Orsay, France, as a Research Fellow. Since 2006, he has been with the Technical University of Belfort-Montbeliard, Belfort, France, as a Lecturer in Control Engineering. His current research interests include automotive and fuel cell control systems, renewable and smart energy management, and power systems.

Dr. Laghrouche has participated in several national and European projects and has the experience of working with global and leading industrial partners.

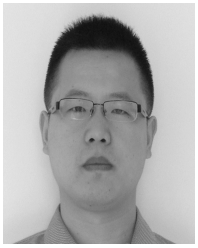

Jianxing Liu was born in Zhejiang, China, in 1986. He received the B.S. and M.S. degrees from the Harbin Institute of Technology, Harbin, China, in 2008 and 2010, respectively, and the Ph.D. degree from the Technical University of Belfort-Montbeliard, Belfort, France, in 2014.

His current research interests include renewable energies, fault diagnosis and identification, and sliding mode control.

Fayez Shakil Ahmed received the Engineering degree in electronics from UIT-Hamdard University, Karachi, Pakistan, in 2005, and the Ph.D. degree from the Technical University of Belfort-Montbeliard, Belfort, France, in 2013.

He has been with the Laboratory of Control and Process Engineering, University Claude Bernard Lyon 1, Villeurbanne, France, since September 2014. He specializes in mechatronics and nonlinear control and observation. His current research interests include embedded systems, industrial electronics, automation systems, and smart energy solutions.

Mohamed Harmouche received the Engineering degree in electronics and control from Al-Jâmi'ah Al-Lubnaniya, Lebanon, in 2006, and the Ph.D. degree from the Technical University of Belfort-Montbeliard (UTBM), Belfort, France, in 2013.

He was an Automation Engineer at SAS Systems, Jeddah, Saudi Arabia, until 2008. He was a Research Engineer with the IRTES-SET Laboratory, UTBM, in 2010. He is currently an Automation and Instrumentation Project Leader with Actility, Paris, France. His current research interests include robust control and observation, machine-to-machine interfaces, and Internet-of-Things in the context of Industry 4.0.

Maxime Wack is currently an Associate Professor with the Technical University of Belfort-Montbeliard, Belfort, France, where he heads the Geopositioning, Embedded Systems, and Mobility Team. His current research interests include intelligent transportation systems, location-based services, and distributed systems.